Indications of Phonon Hydrodynamics in Telescopic Silicon Nanowires

Claudio Melis,[1] Riccardo Rurali,[2] Xavier Cartoixà,[3] and F. Xavier Alvarez[4,*]

[1] *Dipartimento di Fisica, Università di Cagliari, Cittadella Universitaria, 09042 Monserrato, Cagliari, Italy*
[2] *Institut de Ciència de Materials de Barcelona (ICMAB-CSIC), Campus de Bellaterra, 08193 Bellaterra, Catalonia, Spain*
[3] *Departament d'Enginyeria Electrònica, Universitat Autònoma de Barcelona, 08193 Bellaterra, Catalonia, Spain*
[4] *Departament de Física, Universitat Autònoma de Barcelona, 08193 Bellaterra, Catalonia, Spain*

(Received 27 August 2018; revised manuscript received 25 February 2019; published 22 May 2019; corrected 19 June 2019)

The validity of Fourier's law in telescopic nanowires is tested by means of molecular dynamics simulations. We observe that the radial dependence of the heat-flux profile, the temperature jump, and the appearance of vorticity obtained in molecular dynamics telescopic wires near the contact point acquire a hydrodynamic character, and we show that they are incompatible with Fourier's law. We propose the Guyer-Krumhansl equation as a generalization capable of capturing these hydrodynamic effects. Lattice-dynamics results show that the thermal average of the confined modes shows no radial dependence of the vibrating energy inside the wire. This means that hydrodynamic effects could not be related to the confinement effects in these small systems.

DOI: 10.1103/PhysRevApplied.11.054059

I. INTRODUCTION

Fourier's law has been ubiquitously used in the last decades, with the only caveat that the thermal conductivity of a sample may depend on its characteristic size. In simple systems such as nanowires or thin films this means that the thermal conductivity should be calculated from combinations of the intrinsic relaxation times and the sample size through the use of the Mathiessen rule, which states the additivity of the collision frequencies. However the limitations of this Fourier-Mathiessen model (FMM) are twofold. On the one hand calculations from first principles do not show the same size dependence as the experimental measurements [1]. On the other hand, the models cannot reproduce the time and space evolution of temperature profiles using optical setups, even with fitted values of the thermal conductivity [2].

Recent studies have proposed phonon hydrodynamics as the generalization of the more-conventional picture based on Fourier's law suitable for the description of thermal transport at the nanoscale [2–6]. Phonon hydrodynamics is based on the inclusion of memory and nonlocal effects to describe heat dynamics. These are a direct consequence of the presence of conservation of momentum in the sample and can be derived from the Boltzmann transport equation through the changes that this conserved magnitude has on the phonon collision term [7,8]. The direct conservation of momentum in normal collisions [7] or the lack of resistive collisions able to destroy it [8] results in the need to use second-order moments of the distribution function, giving the transport law a form similar to the Navier-Stokes equation [7]. The new phenomenology introduced by these terms enriches the scope and allows deeper insight in the interpretation of experimental results. The presence of phonon hydrodynamics has been observed experimentally through the differences in the thermal maps obtained from heating lines over different substrates and through the size dependence of the thermal conductivity of nanoscale samples [2,6].

Having a proper model to describe heat transport is more important than simply a question of predictability. The equations that we use to simulate an experiment set the phenomenology allowed for its physical interpretation. Fitting a parameter within an incomplete theoretical framework can give wrong information about what is actually happening in the sample. This is key in the design of current nanoscale devices, as the magnitude of properties such as the thermal conductivity used to fit to the experimental data are afterwards used to infer information about individual phonons. Use of a Fourier law when phonon hydrodynamic effects might be present could lead one to wrongly attribute to a change in the phonon relaxation times an effect coming from the presence of memory or nonlocalities in the heat behavior, with the potential risk of misrepresention.

Recent experiments using Fourier's law led to the proposal of an anisotropic thermal conductivity for silicon [9] or the suppression of phonons in bulk samples [10].

*xavier.alvarez@uab.cat

 © 2019 American Physical Society

Both conclusions are difficult to understand if one takes them at face value, but the new framework offers a way to understand them as a consequence of adhering to an effective Fourier framework to interpret hydrodynamic effects. Despite the presence of hydrodynamic effects being widely accepted in two-dimensional materials such as graphene [4,11] or black phosphorus [12], their presence in three-dimensional materials such as silicon is still debated, despite recent experimental observations attributed to Poiseuille flow in $SrTiO_3$ at low temperature [13]. Unfortunately, the lack of access to the microscopic information in the experimental setups does not always allow one to discriminate between the two alternative interpretations. Molecular dynamics (MD) studies can be used to bridge this gap as they have the advantage of providing full control over the atomic scale geometry and composition of the nanowires, as well as having direct access to the time-resolved positions and velocities of the component atoms, which are known at every time step. This allows comparison with theoretical models, which cannot currently be achieved with experiments, while within the computational experiments reported here more detailed time- and space-resolved information such as the local heat flux and the temperature inside the samples can be extracted in a straightforward way.

In this paper we use MD simulations to show that properly accounting for phonon hydrodynamic effects results in a more accurate theoretical framework than the FMM to describe nanoscale thermal transport. We do this by comparing the temperature and heat-flux profiles obtained from nonequilibrium-molecular dynamics (NEMD) computational experiments in nanowires with the predictions of theories that allow for phonon hydrodynamics or stick to the FMM.

II. THEORETICAL BACKGROUND

Fourier's law using a size-dependent thermal conductivity is given by

$$\mathbf{q} = -\kappa_{\text{eff}}(L)\nabla T, \tag{1}$$

where T is the temperature, $\mathbf{q}$ is the heat flux, and $\kappa_{\text{eff}}(L)$ is an effective thermal conductivity that may depend on the sample characteristic length L. To solve this equation, the only boundary conditions that should be given are those of the imposed temperature.

Equation (1) is based on a local-equilibrium hypothesis, but it should be generalized when nonlocal effects are important. The kinetic collective model has been developed to do this in terms of the number of relevant moments of the distribution function [14]. When the difference with respect to equilibrium is reduced to the first moment, the Guyer-Krumhansl (GK) equation can be used [7]:

$$\mathbf{q} = -\kappa\nabla T + \ell^2\nabla^2\mathbf{q} \tag{2}$$

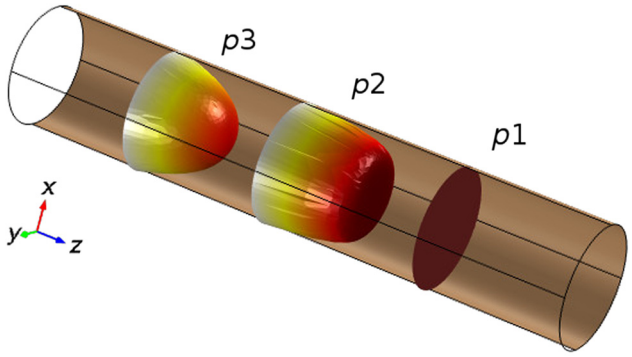

FIG. 1. Heat-flux profiles according to the FMM (p1), the GK equation with $\ell < R$ (p2), and the GK equation with $\ell > R$ (p3).

where ℓ is the nonlocal length that describes the spatial range where momentum conservation has an impact on the phonon distribution. Unlike Fourier's law, this equation is second order in space derivatives and, analogously to the case of temperature, proper boundary conditions for the heat flux should also be given. In this work, we use the Maxwell condition, taken from standard hydrodynamics:

$$\mathbf{q} = -C\ell\frac{d\mathbf{q}}{d\hat{\boldsymbol{n}}}, \tag{3}$$

where $\hat{\boldsymbol{n}}$ is the unit vector in the direction perpendicular to the boundary surface and C is a parameter indicating a reduction of the flux on the boundary. This parameter can be related to the surface roughness, but it can also be related to the enhancement of the anharmonicity of the surface atoms. When $C = 0$, the flow in the boundary is completely suppressed, while for $C > 0$, a surface flow parallel to the boundary is allowed. Finally, we note that the Fourier transform of Eq. (2) is equivalent to a nonlocal kernel of the thermal conductivity described in Ref. [15].

The FMM given by Eq. (1) and the GK model given by Eqs. (2) and (3) give similar results in large systems ($L \gg \ell$) but yield completely different heat profiles for systems with characteristic lengths smaller than the nonlocal length ($L < \ell$). The differences are not only in the effective conductivities but also in the heat-flux profiles obtained. This can be observed when one is solving the two equations for a nanowire whose ends are coupled to thermal baths; see Fig. 1.

We show in Fig. 1 the results for the heat flow along the axial direction for a cross section of a wire using Fourier's law (heat-flux profile p1) and for the hydrodynamic equation for two different values of the nonlocal length ℓ and $C = 0$ (heat-flux profiles p2 and p3). Notice that while the FMM profile is completely flat over the entire cross section, the hydrodynamic profiles are curved, and thus this feature is one of the characteristic signatures of a hydrodynamic transport regime.

The effect of the nonlocal length ℓ in the GK equation can be understood by comparing p2 and p3. In p2, the nonlocal length is shorter than the wire diameter ($\ell < R$). In that case an outer shell where the flux is reduced can be observed, as well as a central flat region in brown where the flux is the same as that of the FMM. In p3 the nonlocal length is greater than the wire radius ($\ell > R$), the central flat region has disappeared, and the region where the boundary is noticed covers all the cross section of the wire, leading to a wholly curved profile. Given that in bulk Si the intrinsic ℓ is approximately 180 nm [16], we expect hydrodynamic effects to manifest themselves at similar or smaller length scales, which is why in the present work we address nanowires of small diameters. Another important effect of the nonlocal term in Eq. (2) is that it introduces vorticity in the heat flux, meaning that the flux direction and the gradient of temperature cease to be parallel. This manifests itself more strongly in situations where the heat flux must make abrupt turns, such as in structures with a sudden change of diameter, nanoconstrictions, and strong bends. These two considerations lead us naturally to the study of telescopic one-dimensional structures [17]. These telescopic one-dimensional systems have been shown to exhibit some promising features as thermal diodes [18]. Larger-scale telescopic nanowires with a similar level of complexity and sharpness of diameter changes have also been reported experimentally [19]. The sharpness of the constriction plays a central role with respect to the phenomenology of the heat flux described here and this is the reason why the abrupt telescopic junction that we consider is a suitable system to study these effects. For these effects to manifest themselves, the curvature radius of the junction should be less than the nonlocal length ℓ.

Therefore, NEMD simulations are performed on telescopic Si nanowires grown along the [111] direction, with a steplike variation of the diameter changing from $d_1 = 5$ nm to $d_2 = 10$ nm and a total length $L = 60$ nm (see Fig. 2). We perform NEMD simulations with the LAMMPS code [20], using a Stillinger-Weber potential [21] reparameterized with a first-principles-based force-matching method that relies on density-functional calculations of the restoring forces for atomic displacements [22]. This new set of parameters increases the predictive power of the thermal conductivity of the interatomic potential (see Ref. [22] for more details). The energy per unit time emitted or absorbed by the hot and cold reservoirs is monitored as the steady state is approached, considering that the system is stationary when the two magnitudes are within 0.5%. We take $\Delta T = 400$ K with ($T_{\text{cold}} = 100$ K), in line with typical NEMD simulations [23,24]. The use of the large temperature gradients associated with NEMD simulations was validated against equilibrium Green-Kubo calculations to obtain lattice thermal conductivity in bulk Si [23] and more recently for nanoscale Si [25]. A lower temperature difference between the hot and cold reservoirs would result in more-realistic thermal gradients, but at the same time would require much longer simulation times to equilibrate the system. Despite this, the qualitative behavior of the heat flux is not expected to change significantly.

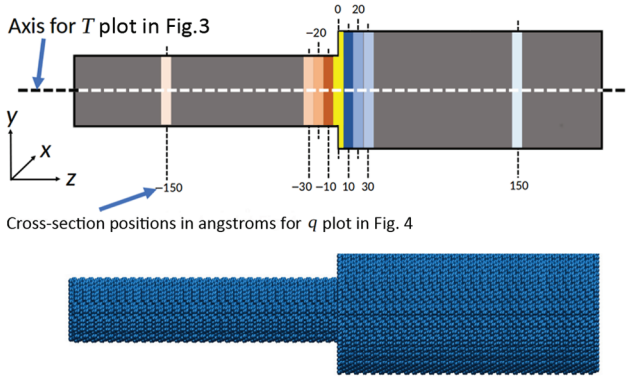

FIG. 2. Axial cross section of the system studied and the different sections used to study the heat-flux profile.

We perform 22×10^6 NEMD steps with a time step of 0.7 fs and average the local heat fluxes over the last 15×10^6 steps. During this interval, the heat flux is sampled on each lattice site according to the standard definition [26]

$$\boldsymbol{J}_i = e_i \boldsymbol{v}_i - \overline{\overline{S}}_i \boldsymbol{v}_i \tag{4}$$

where e_i is the energy per atom (potential and kinetic), $\boldsymbol{v}_i$ is the velocity, and $\overline{\overline{S}}_i$ is the stress tensor. The heat flux per atom $\boldsymbol{J}_i$ is time averaged for the final interval of 15×10^6 MD steps and then spatially averaged over eight cylindrical shells (four in the case of the inner wire) centered at the wire axis each one having a thickness of 0.6 nm. The spatial average is obtained by our summing $\boldsymbol{J}_i$ for all the atoms belonging to a specific cylindrical shell and dividing the sum by the corresponding volume.

III. RESULTS AND DISCUSSION

The temperature and heat-flux profiles obtained in the MD simulations are shown in Figs. 3 and 4, where the error bars represent the standard deviation corresponding to the time average. To compare the suitability of the models, we obtain the best-fitting results for these data from the FMM and the GK equationsolved through the finite-element method using COMSOL MULTIPHYSICS. For the FMM we perform fitting with an effective thermal conductivity for the two different sections, obtaining $\kappa = 32$ W/mK for the $d_1 = 5$ nm section and $\kappa = 45$ W/mK for the $d_2 = 10$ nm section. For the GK model, we adjust the values of the three parameters that appear in Eqs. (2) and (3). Two of them (C and ℓ) have an effect on the form of the curved profile, while κ has an effect only on the height of the profile. The results for the fitting are

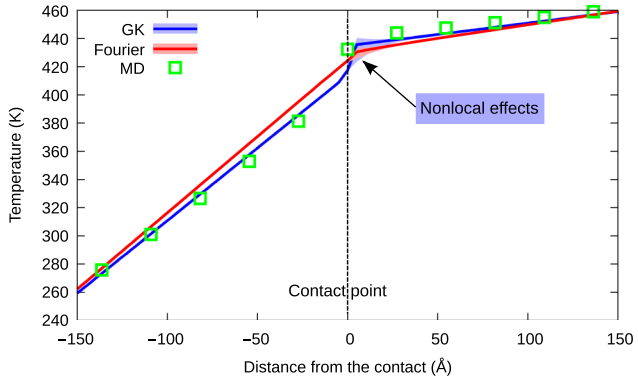

FIG. 3. Temperature profiles along the axis. Notice that the hydrodynamic models have a steeper decrease at the contact point due to the effect of the nonlocal term.

$\ell = 0.5$ nm and $\kappa = 37$ W/mK for the $d_1 = 5$ nm section and $\ell = 2$ nm and $\kappa = 80$ W/mK for the $d_2 = 10$ nm section. A fitted value of $C = 0.4$ is used for both sections, indicating the enhancement of anharmonic effects at the nanowire surface. Although the kinetic collective model allows the calculation of ℓ and κ from scattering rates obtained from first principles, this procedure is not possible in this case due to the size of the wires, which is small enough to affect the phonon density of states, so bulk figures cannot be used, but is too large to be treated *ab initio*.

The first evidence of a hydrodynamic behavior can be observed in Fig. 3. The temperature profile along the axis is represented near the telescopic contact. The points represent the MD averaged temperatures on slices of the structure at different axial positions. The solid lines are the FMM and GK averaged temperatures on a cross section and the shaded regions indicate the temperature variation over them. This variation is a consequence of the spreading of flux near the contact point in passing from the small-diameter section to the large-diameter section. It can be observed that MD results predict a temperature jump at that point. Using a FMM this behavior can be obtained only with the addition of a supplementary thermal boundary resistance (TBR). Without it, as we have here, the solution passes simply from one slope to another because of the change in the thermal conductivity, but no transition is predicted. Notice that in the FMM the variation of the temperature in the cross direction does not affect its mean value. In contrast, the nonlocal term in the GK equation has an effect on the averaged temperature. In the regions where the heat flux spreads, the Laplacian term in Eq. (2) becomes important. This term is the responsible for an increase of the local resistivity, which is understandable from the observation that in the Navier-Stokes equation this term introduces a viscous effect. The consequence is a steeper slope of the temperature, similar to that obtained with a TBR.

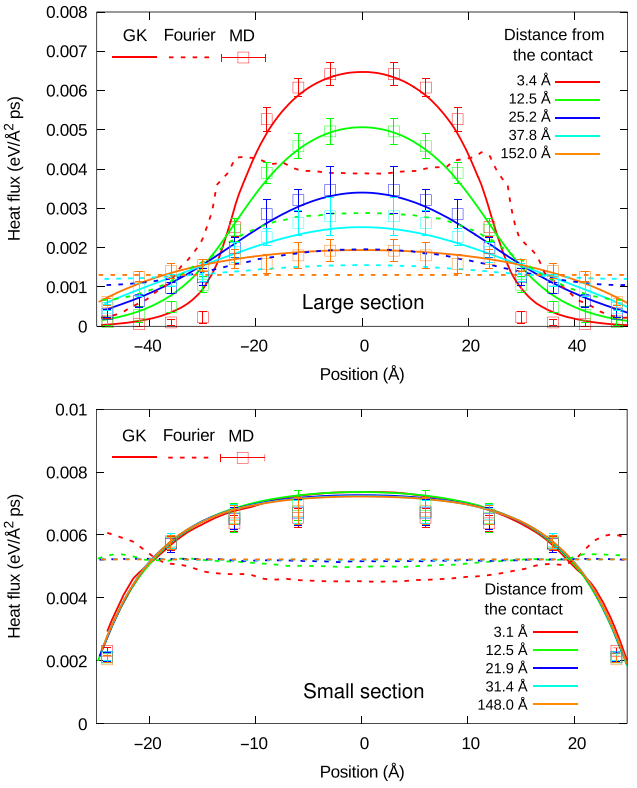

FIG. 4. Flux profiles obtained from MD simulations, the FMM, and the GK equation for large (top) and small (bottom) sections of the telescopic wire.

Of course, a physical contribution to the TBR coming from the difference in the dispersion relations in the constituent nanowires could also be present in the MD results, but the GK equation is able to naturally capture a significant part of the effect in our system. A dependence of TBR in terms of the characteristic size has been proposed in some experimental studies to explain, from a FMM, the observed reduction of the effective thermal conductivity in some devices [27]. Here we propose that the nonlocal effects appearing in the GK model could offer a complementary explanation for this observation.

Further evidence can be observed in Fig. 4, where the obtained average flux as a function of the radial distance is represented for the different regions. A curved profile is obtained, where near the axis of the wire the heat flow is greater than at the wire boundary. The FMM predictions (dotted lines) for the flux are significantly different. In the central part of the wire (15 nm from the contact point), the heat profile obtained is flat (i.e., independent of the radial position). The lack of control over the heat flux at the boundaries means that the only way to obtain this result is by use of a thermal conductivity depending on the radial position. With use of the GK equation (solid lines), this behavior is naturally obtained. Besides, near the contact, the GK equation and MD simulations give a similar

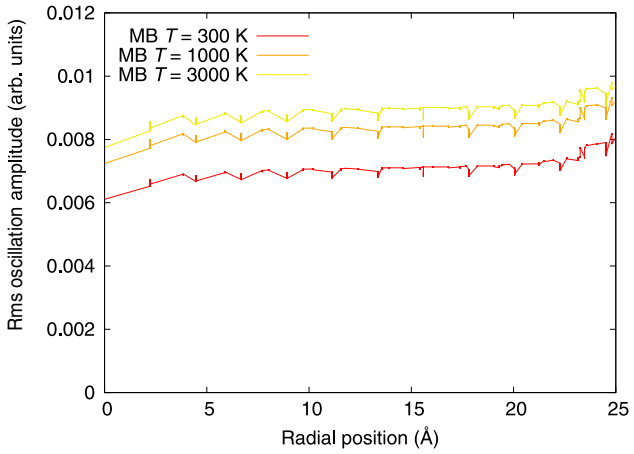

FIG. 5. Oscillation-amplitude profile from lattice dynamics. The amplitudes of the eigenmodes weighted by a thermal occupation factor are summed. It can be observed that the oscillation amplitude cannot offer an explanation for the reduced flux obtained in MD simulations at the boundaries. MB, Maxwell-Boltzmann.

smooth transition of the heat flux from the thin to the thick wire, while the FMM predicts an increase of the flux near the boundaries in clear opposition to the MD results.

The usual justification for the radial dependence of the heat flow is based on the boundary collisions of the phonons. Heat flow is suppressed at the boundary, and this is noticed only in a Knudsen layer inside the system. But in the case that we are studying, this reason is not clearly justified. The radial size of the wire is small enough for us to think that we are in the presence of heat carrier confinement, given that it is much less than typical phonon mean free paths. In that case, modes are stationary in the cross section and they propagate only along the axial direction.

To have stronger evidence that the surface reduction of the heat flux does not come from the vibrational amplitude profile of the lattice, we calculate the oscillation amplitude of the atoms as a function of the radial position using lattice dynamics for the wire with $d_1 = 5$ nm. For this we start from a unit cell of 926 atoms, which is the minimal structure that is repeated along the z direction, where we use periodic boundary conditions. Once we have the modes after the diagonalization of the corresponding dynamical matrix, we sum the rms thermal amplitudes [28] using the Maxwell-Boltzmann factor. The results are shown in Fig. 5. Notice that the rms-thermal-amplitude profile is fairly constant along the radial direction, with an increase near the surface due to the effects of weaker bonding, showing that the reduction of the heat flux at the edge cannot be expected from the differences in the amplitudes of the vibrational modes.

Further evidence is the vorticity near the step region. Figure 6 shows the computed temperature gradient and local heat flux in region 1 of the structure, where it is observed that, as allowed by Eq. (2), the two vectors are not collinear. To have this behavior in a pure Fourier law, one must resort to a tensor (i.e., anisotropic) thermal conductivity. This anisotropicity in κ has been invoked to explain the findings of some experiments where fittings for the in-plane and through-plane thermal conductivities using Fourier's law in a Si wafer yielded values as different as 80 and 140 W/mK, respectively [9], but werecently showed that Eq. (2) can also explain the experimental results while keeping the isotropic character of the thermal conductivity in bulk Si at mesoscopic length scales [6].

IV. CONCLUSIONS

We show, by means of molecular dynamics simulations, that deeply scaled telescopic silicon nanowires feature

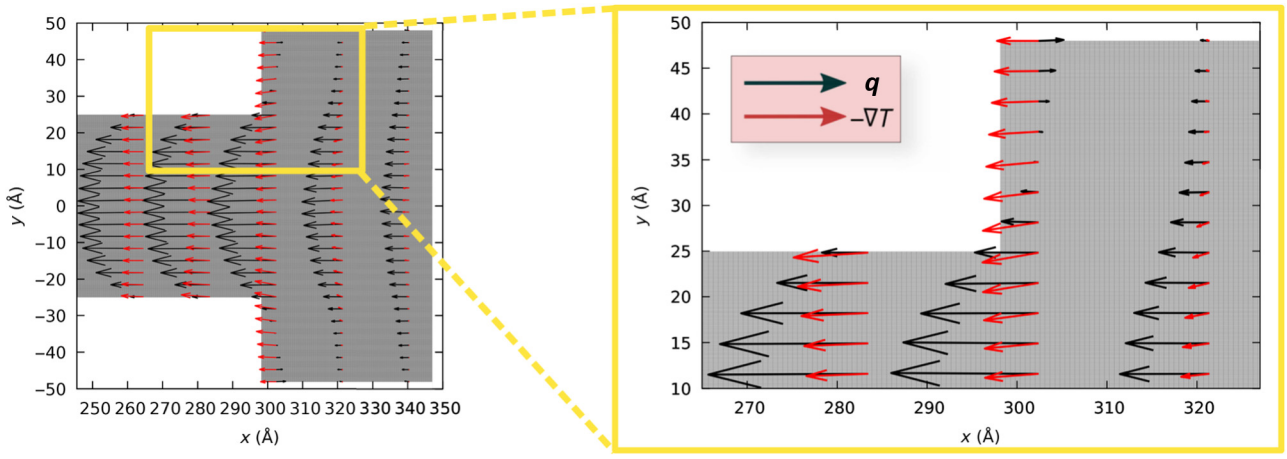

FIG. 6. Averaged temperature gradient (red arrows) and heat flux (black arrows) obtained from the postprocessing of the NEMD simulations. It is observed that the two are not collinear.

signatures of hydrodynamic effects; namely, a drag at the surface in the heat flux, the appearance of a steep slope in the interface region analogous to a thermal boundary resistance, and a vorticity. These effects are straightforwardly explained by the GK equation, which adds a hydrodynamic term to the heat-flux constitutive law. These results could have a big impact in the engineering and applied physics communities as the behavior of thermal transport at the extremely reduced scales of current electronic devices can be largely influenced by the appearance of viscous and vorticity effects shown in this work. Taking into consideration these effects in the design stage could be key to improving the performance of these devices.

ACKNOWLEDGMENTS

We very gratefully acknowledge Professor Luciano Colombo's critical reading of the manuscript. We also acknowledge financial support by the Ministerio de Economía, Industria y Competitividad (MINECO) under Grants No. FEDER-MAT2013-40581-P, No. TEC2015-67462-C2-2-R (MINECO/FEDER), and No. TEC2015-67462-C2-1-R (MINECO/FEDER), by the Severo Ochoa Centers of Excellence Program under Grant No. SEV-2015-0496, and by the Generalitat de Catalunya under Grant No. 2014 SGR 301.

[1] Wu Li and Natalio Mingo, Thermal conductivity of diamond nanowires from first principles, Phys. Rev. B **85**, 195436 (2012).

[2] Amirkoushyar Ziabari, Pol Torres, Bjorn Vermeersch, Yi Xuan, Xavier Cartoixà, Alvar Torelló, Je-Hyeong Bahk, Yee Rui Koh, Maryam Parsa, Peide D. Ye, F. Xavier Alvarez, and Ali Shakouri, Full-field thermal imaging of quasiballistic crosstalk reduction in nanoscale devices, Nat. Commun. **9**, 255 (2018).

[3] F. X. Alvarez, D. Jou, and A. Sellitto, Phonon hydrodynamics and phonon-boundary scattering in nanosystems, J. Appl. Phys. **105**, 014317 (2009).

[4] A. Cepellotti, G. Fugallo, L. Paulatto, M. Lazzeri, F. Mauri, and N. Marzari, Phonon hydrodynamics in two-dimensional materials, Nat. Commun. **6**, 6400 (2015).

[5] Andrea Cepellotti and Nicola Marzari, Boltzmann transport in nanostructures as a friction effect, Nano Lett. **17**, 4675 (2017).

[6] P. Torres, A. Ziabari, A. Torelló, J. Bafaluy, J. Camacho, X. Cartoixà, A. Shakouri, and F. X. Alvarez, Emergence of hydrodynamic heat transport in semiconductors at the nanoscale, Phys. Rev. Mater. **2**, 076001 (2018).

[7] R. A. Guyer and J. A. Krumhansl, Solution of the linearized phonon Boltzmann equation, Phys. Rev. **148**, 766 (1966).

[8] Yangyu Guo and Moran Wang, Phonon hydrodynamics for nanoscale heat transport at ordinary temperatures, Phys. Rev. B **97**, 035421 (2018).

[9] R. B. Wilson and D. G. Cahill, Anisotropic failure of Fourier theory in time-domain thermoreflectance experiments, Nat. Commun. **5**, 5075 (2014).

[10] Jeremy A. Johnson, A. A. Maznev, John Cuffe, Jeffrey K. Eliason, Austin J. Minnich, Timothy Kehoe, Clivia M. Sotomayor Torres, Gang Chen, and Keith A. Nelson, Direct Measurement of Room-Temperature Nondiffusive Thermal Transport over Micron Distances in a Silicon Membrane, Phys. Rev. Lett. **110**, 025901 (2013).

[11] Sangyeop Lee, David A. Broido, Keivan Esfarjani, and Gang Chen, Hydrodynamic phonon transport in suspended graphene, Nat. Commun. **6**, 6290 (2015).

[12] Yo Machida, Alaska Subedi, Kazuto Akiba, Atsushi Miyake, Masashi Tokunaga, Yuichi Akahama, Koichi Izawa, and Kamran Behnia, Observation of Poiseuille flow of phonons in black phosphorus, Sci. Adv. **4**, eaat3374 (2018).

[13] Valentina Martelli, Julio Larrea Jiménez, Mucio Continentino, Elisa Baggio-Saitovitch, and Kamran Behnia, Thermal Transport and Phonon Hydrodynamics in Strontium Titanate, Phys. Rev. Lett. **120**, 125901 (2018).

[14] C. de Tomas, A. Cantarero, A. F. Lopeandia, and F. X. Alvarez, From kinetic to collective behavior in thermal transport on semiconductors and semiconductor nanostructures, J. Appl. Phys. **115**, 164314 (2014).

[15] Philip B. Allen, Analysis of nonlocal phonon thermal conductivity simulations showing the ballistic to diffusive crossover, Phys. Rev. B **97**, 134307 (2018).

[16] P. Torres, A. Torelló, J. Bafaluy, J. Camacho, X. Cartoixà, and F. X. Alvarez, First principles kinetic-collective thermal conductivity of semiconductors, Phys. Rev. B **95**, 165407 (2017).

[17] T. I. Kamins, X. Li, and R. Stanley Williams, Thermal stability of Ti-catalyzed Si nanowires, Appl. Phys. Lett. **82**, 263 (2003).

[18] Xavier Cartoixà, Luciano Colombo, and Riccardo Rurali, Thermal rectification by design in telescopic Si nanowires, Nano Lett. **15**, 8255 (2015).

[19] Joseph D. Christesen, Christopher W. Pinion, Erik M. Grumstrup, John M. Papanikolas, and James F. Cahoon, Synthetically encoding 10 nm morphology in silicon nanowires, Nano Lett. **13**, 6281 (2013).

[20] Steve Plimpton, Fast parallel algorithms for short-range molecular dynamics, J. Comp. Phys. **117**, 1 (1995).

[21] Frank H. Stillinger and Thomas A. Weber, Computer simulation of local order in condensed phases of silicon, Phys. Rev. B **31**, 5262 (1985).

[22] Yongjin Lee and Gyeong S. Hwang, Force-matching-based parameterization of the Stillinger-Weber potential for thermal conduction in silicon, Phys. Rev. B **85**, 125204 (2012).

[23] Patrick K. Schelling, Simon R. Phillpot, and Pawel Keblinski, Comparison of atomic-level simulation methods for computing thermal conductivity, Phys. Rev. B **65**, 144306 (2002).

[24] David G. Cahill, Wayne K. Ford, Kenneth E. Goodson, Gerald D. Mahan, Arun Majumdar, Humphrey J. Maris, Roberto Merlin, and Simon R. Phillpot, Nanoscale thermal transport, J. Appl. Phys. **93**, 793 (2003).

[25] Haikuan Dong, Zheyong Fan, Libin Shi, Ari Harju, and Tapio Ala-Nissila, Equivalence of the equilibrium and the nonequilibrium molecular dynamics methods for thermal conductivity calculations: From bulk to nanowire silicon, Phys. Rev. B **97**, 094305 (2018).

[26] Robert J. Hardy, Energy-flux operator for a lattice, Phys. Rev. **132**, 168 (1963).

[27] Mark E. Siemens, Qing Li, Ronggui Yang, Keith A. Nelson, Erik H. Anderson, Margaret M. Murnane, and Henry C. Kapteyn, Quasi-ballistic thermal transport from nanoscale interfaces observed using ultrafast coherent soft X-ray beams, Nat. Mater. **9**, 26 (2010).

[28] Atsushi Togo and Isao Tanaka, First principles phonon calculations in materials science, Scr. Mater. **108**, 1 (2015).

Correction: Figure 4 was processed improperly during the initial production cycle and has been fixed.